

Granular rotor as a probe for a non-equilibrium bath

Tomohiko G. Sano¹, Kiyoshi Kanazawa², and Hisao Hayakawa¹

¹*Yukawa Institute for Theoretical Physics, Kyoto University,
Kitashirakawa-oiwake cho, Sakyo-ku, Kyoto 606-8502, Japan*

²*Department of Computational Intelligence and Systems Science,
Interdisciplinary Graduate School of Science and Engineering, Tokyo Institute of Technology,
4259-G3-52 Nagatsuta-cho, Midori-ku, Yokohama 226-8503, Japan*

The dynamics of a rotor under viscous or dry friction is investigated as a non-equilibrium probe of a granular gas numerically and analytically. To demonstrate a role of the rotor as a probe for a non-equilibrium bath, we perform the molecular dynamics (MD) simulation of the rotor under viscous or dry friction surrounded by a steady granular gas under gravity. We theoretically derive a one-to-one map between the velocity distribution function (VDF) for the granular gas and the angular one for the rotor. With the aid of the MD simulation, we demonstrate that the one-to-one map works well to infer the local VDF of the granular gas from the angular one of the rotor, and vice versa.

PACS numbers: 45.70.-n, 05.40.Fb, 05.20.Dd, 05.10.Gg

I. INTRODUCTION

Temperature is one of the most important quantities in equilibrium thermodynamics [1, 2]. One can generalize the concept of temperature to characterize various non-equilibrium systems. Although many authors have proposed non-equilibrium temperatures, their validity has not been sufficiently clarified so far [3–5]. Indeed, there are some reports that the effective temperatures in non-equilibrium systems do not satisfy the fundamental laws of thermodynamics, such as the zeroth law [6–10].

There are many attempts to introduce effective temperatures even for granular systems [11–14]. One of the most famous ones is the Edwards temperature, which is associated with the compactivity and is mainly used for static ensembles of granular particles [15–22]. Another well-known temperature is the kinetic temperature or the granular temperature, which is the second-order cumulant of the velocity distribution function (VDF) and is related to the kinetic energy of granular particles [23–39]. The latter effective temperature is appropriate in describing the granular flows even in the vicinity of jamming transition, whereas we do not have the consensus of what temperature is useful for general setups of granular systems [36–39]. Moreover, we have to take into account the effects of higher-order cumulants explicitly to characterize granular assemblies, because granular assemblies have non-Maxwellian nature of the VDF, i.e., the existence of higher-order cumulants [10, 40–43]. We also indicate that a measurement probe plays an important role in non-equilibrium systems. In particular, the granular temperature and higher-order cumulants for granular assemblies should be inferred from the measurement of the motion of the probe.

For local thermal equilibrium gases, the local temperature can be measured through the observation of the motion of a Brownian tracer, because the second cumulant of the VDF of the tracer is directly related to the temperature according to the fluctuation-dissipation re-

lation. On the other hand, it is nontrivial whether we can infer the distributions of non-equilibrium environments only observing the motion of the tracer attached to environments such as granular gases [44, 45]. Kanazawa *et al.* suggested that such a characterization is possible through the analysis of a non-Gaussian Langevin equation [46, 47], where an inverse estimation formula is derived to infer the non-equilibrium granular VDF from the observation of the tracer. Although the usefulness of the inverse formula has already been numerically verified on the basis of the Boltzmann-Lorentz equation for spatially homogeneous and isotropic granular gases [48–54], the model may not be sufficiently realistic because inhomogeneity and anisotropy exist in real granular gases such as vertically vibrated granular systems under gravity [41]. This implies that more realistic formulation is necessary for experimental measurement of high-order cumulants by observation of the tracer dynamics.

In this paper, the molecular dynamics (MD) simulation of a realistic granular rotor is performed to demonstrate the role of a rotor as a probe to measure the VDFs of vibrating granular beds [55–60]. We perform an event driven MD simulation of a rotating rotor around a fixed axis in a vertically vibrated granular gas under gravity as in Ref. [13]. We numerically find that non-Gaussian VDFs for granular gases are cylindrically symmetric. We analyze the dynamics of the rotor in vibrating granular beds to derive the relationship between the angular VDF of the rotor under viscous or dry friction and the VDF of the granular gas [46, 47]. We demonstrate that the angular VDF of the rotor is correctly predicted from the VDFs of the granular gas, and is vice versa using our derived formulas. Because the motion of the rotor in vibrating beds can be easily observed in experiments, our method is, in particular, useful in the following two situations: Experiments for both vibrating granular gases deep inside a three dimensional container and the gases in an opaque container. Furthermore, we demonstrate that our formulas are valid even for the rotor near the

boundary of the container. We thus indicate that the granular rotor under viscous or dry friction can be used as a local probe for a realistic granular gas.

The organization of this paper is as follows. We explain the setup of our simulation in Sec. II and show that the VDF for granular gases is cylindrically symmetric. In Sec. III, we briefly explain the theoretical setup to derive the inverse formula for the cylindrically symmetric granular gas [46, 47]. In Sec. IV, we show the existence of formulas between the VDF for the gas and the angular VDF for a rotor under a viscous friction around a rotating axis. The validity of these formulas is also numerically verified in this section. In Sec. V, we discuss the position dependence of the viscous rotor. In Sec. VI, we examine the angular VDF for a dry frictional rotor using the numerical VDF for the granular gas under gravity. In Sec. VII, we conclude this paper with some remarks. In Appendix. A, we examine the rotor under viscous friction in an elastic gas without gravity as a benchmark test of our simulation and formulation, where the angular VDF for the rotor is analytically obtained. In Appendices B and D, we show the detailed calculation of our analytic formulas for the viscous and dry frictional rotors, respectively. We explain the detailed procedure to apply our formulas to the viscous and dry frictional rotors in Appendices C and E, respectively.

II. SIMULATION SETUP

The schematic figure of our setup is illustrated in Fig. 1. We prepare $N = 100$ frictionless grains of diameter $d = 0.02\sqrt{A}$ and mass m under gravity g in a quasi two-dimensional container (area $A = L_{\text{box}}^2$, height $H_{\text{box}} = 0.1L_{\text{box}}$). The VDF is different from the Gaussian for inelastic grains under gravity and vibration ($e_g < 1$). Following Refs. [61, 62], we adopt $e_g = 0.71$ for inelastic grains, which is the effective restitution coefficient for low density polyethylene. The restitution coefficient between grains and the side wall is chosen to be identical to that for collisions between grains. We do not consider neither the rotational motion of grains nor the tangential contact force between grains in this paper because the effect of the tangential friction of spherical grains can be absorbed into the effective normal restitution coefficient if the duration time of grains is negligible [63–66].

The origin of the system in the laboratory frame $(x, y, z) = (0, 0, 0)$ is chosen to be the bottom center of the container at $t = 0$. We introduce a thin rotor of mass M rotating around the fixed axis $(x, y) = (x_0, y_0)$ under the frictional torque $\hat{N}_{\text{fri}}(\hat{\omega})$ with width $w = 0.1L_{\text{box}}$ and height $h = H_{\text{box}} - d$ (Fig. 2 (a) and (b)). We introduce the restitution coefficient e between the rotor and grains and adopt $e = e_g = 0.71$. The density of the granular gas is $\rho = N/h(L_{\text{box}} - d)^2$. We introduce the typical velocity of grains as $v_0 = \sqrt{gL_{\text{box}}}$. We assume that the rotor is sufficiently macroscopic, i.e., $\epsilon \equiv m/M = 0.01 \ll 1$. The local VDF for the gran-

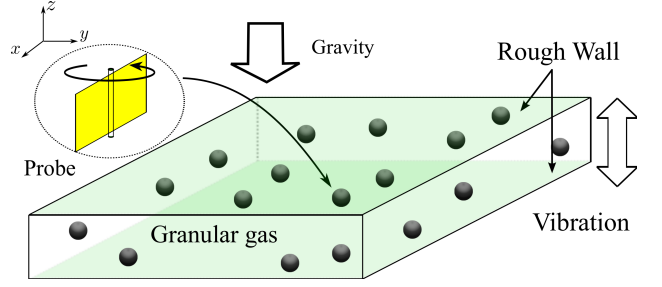


FIG. 1: (Color online) Schematic picture of our simulation.

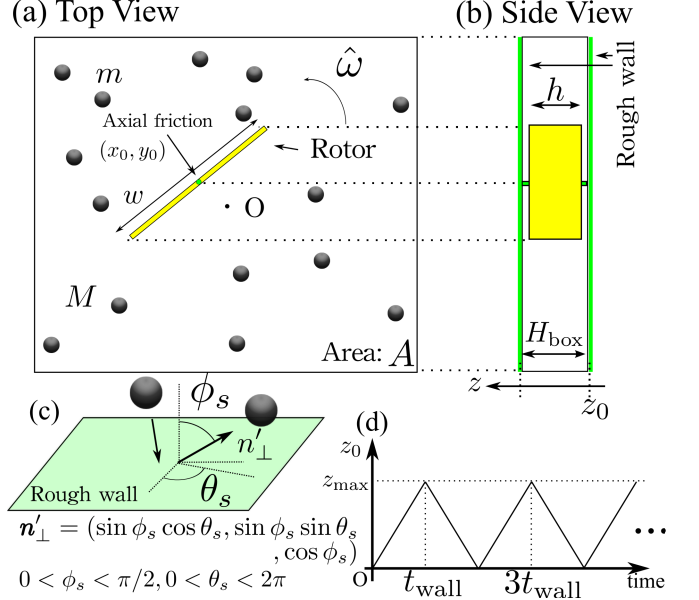


FIG. 2: (Color online) Schematics of (a) the top view and (b) the side view of our simulation. The rotor rotates around a fixed axis (x_0, y_0) , and the origin O is the center of the container. Note that the size of the rotor is exaggerated. (c) The rough wall reflects the grain in random direction. (d) The container is vibrated vertically in a piece-wise linear manner. The time evolution of the bottom of the container is shown.

ular gas is measured near the rotating axis in the region of $r = \sqrt{(x - x_0)^2 + (y - y_0)^2} < r_{\text{obs}} \equiv 2w$ and $z_0 < z < z_0 + H_{\text{box}}$.

Rough walls are introduced both on the top and the bottom of the container to distribute the energy into horizontal direction. (See Fig. 2 (b).) When a grain collides against the rough wall, the post collisional direction \mathbf{n}'_{\perp} is randomized, while the kinetic energy is conserved during the collision. The scattered angles (θ_s, ϕ_s) are chosen from uniform random variables in $0 \leq \phi_s \leq \pi/2, 0 \leq \theta_s \leq 2\pi$. (See Fig. 2 (c).) Note that the probability density per a unit solid angle for small ϕ_s is higher than that for large ϕ_s , while that for the horizontal direction θ_s is uniform. The rough walls correspond to the walls where sandpapers are glued [69]. We

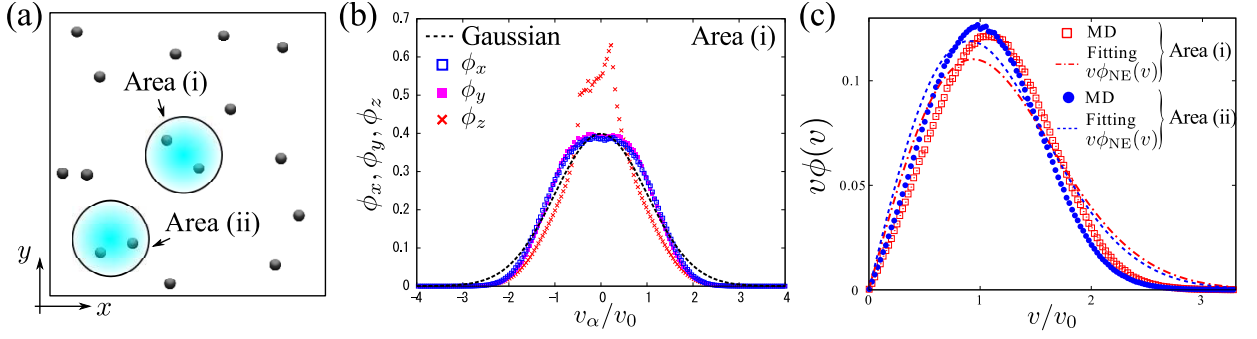


FIG. 3: (Color online) (a): The area (i) is the cylindrical area with the radius r_{obs} around $x = 0, y = 0$, and the area (ii) is the one around $x = -L_{\text{box}}/4, y = -L_{\text{box}}/4$. (b): VDFs for $\alpha = x, y, z$ directions are shown. The data are taken in the area (i). VDFs for horizontal direction are different from Gaussian (dotted line). VDF in z direction is asymmetric due to the gravity. (c): The VDFs for $v = \sqrt{v_x^2 + v_y^2}$ in the areas (i) and (ii) are shown as open squares and filled circles, respectively. It should be noted that the VDF for area (i) differs from that in the area (ii) due to the wall. Our observed VDFs cannot be fitted by the theoretical VDFs in Ref. [25] represented by the chain line and the dashed line for the area (i) and (ii), respectively.

inject energy into the granular gas by vertically vibrating the container in a piece-wise manner with a constant speed [70]. Figure 2 (d) illustrates the time evolution of the bottom wall $z = z_0$. The direction of the container motion is changed every $t_{\text{wall}} = 0.1L_{\text{box}}/v_0$. The maximum height of the bottom is $z_{\text{max}} = 0.02H_{\text{box}}$. It should be stressed that the rough wall is different from the thermal wall, where the magnitude of velocity is randomly chosen from the Maxwell distribution function [67, 68]. See Appendix A for the results of a simulation of grains associated with a thermal wall.

We here emphasize that the VDF for the gas is cylindrically symmetric. We observe the VDF in the two regions; the areas (i) and (ii). Here, the center of the area (i) is $(x, y) = (0, 0)$, and that of the area (ii) is $(x, y) = (-L_{\text{box}}/4, -L_{\text{box}}/4)$ (Fig. 3 (a)). The VDFs ϕ_α for $\alpha = x, y, z$ directions are shown in Fig. 3 (b), where the data are taken in the area (i). We note that VDFs even for horizontal direction deviate from Gaussian (dotted line) $\exp(-x^2/2)/\sqrt{2\pi}$ with $x = v_\alpha/v_0$. Because the rotor rotates around the vertical axis, the axis parallel to the z axis, and the rotor cannot detect VDF for the z direction in our setup, we do not consider the VDF for v_z . Thus, we formulate the inverse formula for cylindrically symmetric gases on the basis of the Boltzmann-Lorentz equation. We have confirmed that the VDFs are invariant whether the rotor is present or not. In Fig. 3 (c), the numerical data of VDFs for $v \equiv \sqrt{v_x^2 + v_y^2}$ are shown for both the areas (i) and (ii). It should be noted that

the VDF in the areas (i) (open squares) differs from that in the area (ii) (filled circles) because of the influence of the wall. In this paper, we consider only the area (i) in Secs. IV and VI, while we discuss the data for both area (i) and (ii) in Sec. V.

Let us compare our obtained VDFs with that for granular gases activated by a white noise thermostat [25], which is phenomenologically used for the analysis of vibrating granular gases [29]. We note that our observed VDFs cannot be fitted by that in Ref. [25], which is written as $\phi_{\text{NE}}(v) = (1 + a_2 S_2(v^2/v_{\text{th}}^2))\phi_G(v/v_{\text{th}})/v_{\text{th}}^2$ with $\phi_G(x) \equiv \exp(-x^2/2)/2\pi$, $a_2 = 16(1 - e_g)(1 - 2e_g^2)/\{185 - 153e_g + 30(1 - e_g)e_g^2\}$, and $S_2(x) = x^2/2 - 2x + 1$. Here, v_{th} corresponds to a fitting parameter in our setup. The fitting results are shown in Fig. 3 (c) and $v_{\text{th}}/v_0 = 0.935587$ and $v_{\text{th}}/v_0 = 0.900656$ for the areas (i) (chain line) and (ii) (dashed line), respectively.

III. THEORETICAL STARTING POINT

We explain our theoretical starting point for the cylindrically symmetric granular gases. We only consider the two-dimensional VDF $\phi = \phi(v_x, v_y)$ for grains to calculate the angular VDF for the rotor. The time evolution of the probability distribution function (PDF) of the angular velocity of the rotor $P = P(\omega, t)$ can be described by the Boltzmann-Lorentz equation [48–54]:

$$\frac{\partial P}{\partial t} + \left\{ \frac{\partial}{\partial \omega} N_{\text{fri}} P \right\} = \int_{-\infty}^{\infty} dy \{ W_\epsilon(\omega - y; y) P(\omega - y, t) - W_\epsilon(\omega; y) P(\omega, t) \}, \quad (1)$$

$$\epsilon W_\epsilon(\omega; y) \equiv \rho h \int_0^{2\pi} d\varrho \int_{-\infty}^{\infty} dv_x dv_y \phi(v_x, v_y) \Theta(V_n(\varrho) - v_n) |V_n(\varrho) - v_n| \delta\left(\frac{y}{\epsilon} - \Delta\bar{\omega}\right). \quad (2)$$

Here, we have introduced $\mathbf{V}(\varrho) \equiv \omega \mathbf{e}_z \times \mathbf{r}(\varrho)$, $\Delta\bar{\omega} \equiv g(\varrho)(1 + e)(V_n - v_n)/\{R_I(1 + \epsilon g^2(\varrho))\}$, $g(\varrho) \equiv r_t(\varrho)/R_I$, $\mathbf{t}(\varrho) \equiv \mathbf{e}_z \times \mathbf{n}(\varrho)$, and $R_I \equiv \sqrt{I/M}$, where \mathbf{n} and \mathbf{t} are normal and tangential unit vectors on the surface of the rotor, respectively. Correspondingly, the variables with subscripts n and t are, respectively, the normal and the tangential components of the variables. Note that such a set of equations is widely used in systems, such as granular gases activated by a white noise thermostat [25, 71–75]. We have also introduced ϱ as a coordinate variable along the surface of the rotor, running over $0 < \varrho < 2w$ [48]. According to Refs. [46, 47], Eq. (1) is reduced to a Langevin equation for $\Omega \equiv \omega/\epsilon$ driven by the state-independent non-Gaussian noise in the large system size limit $\epsilon \rightarrow 0$ when the axial friction is sufficiently strong. In the following, we consider the two types of the axial friction, the viscous friction $N_{\text{fri}} = -\gamma\omega$ and the dry friction $N_{\text{fri}} = -\Delta \text{sgn}(\omega)$, with $\text{sgn}(x) \equiv x/|x|$ and $\text{sgn}(0) = 0$ [76–80], and discuss the steady state distribution $P_{\text{ss}}(\Omega) \equiv \lim_{t \rightarrow \infty} \mathcal{P}(\Omega, t)$ with $\mathcal{P}(\Omega, t) \equiv \epsilon P(\epsilon\Omega, t)$.

IV. GRANULAR ROTOR UNDER VISCOUS FRICTION

In this section, we consider the role of the rotor under viscous friction $N_{\text{fri}} = -\gamma\omega$ as a probe of the granular gas. In Sec. IV A, we analytically derive forward and inverse formulas, which connect the granular VDF with the rotor PDF. In Sec. IV B, we verify the validity of the forward formula at first, where we estimate $P_{\text{ss}}(\Omega)$ using the numerical data for $\phi(v)$. Next, in Sec. IV C, we solve the inverse problem, i.e., we derive the granular VDF $\phi(v)$ from a given $P_{\text{ss}}(\Omega)$, which enables us to infer the properties of granular gases from the motion of the probe, i.e., the rotor.

A. Analytic formula for PDF of the rotor

With the aid of Ref. [81], the steady angular VDF in the Fourier transform $\tilde{P}_{\text{ss}}(s) \equiv \int_{-\infty}^{\infty} d\Omega e^{is\Omega} P_{\text{ss}}(\Omega)$ can be expressed as

$$\tilde{P}_{\text{ss}}(s) = \exp \left[\int_0^s \frac{I}{\gamma s'} \Phi(s') ds' \right], \quad (3)$$

where the cumulant generating function $\Phi(s) \equiv \sum_{l=1}^{\infty} \mathcal{K}_l (is)^l / l! = \int_{-\infty}^{\infty} \mathcal{W}(\mathcal{Y}) (e^{i\mathcal{Y}s} - 1)$ with $\mathcal{K}_l \equiv \int_{-\infty}^{\infty} d\mathcal{Y} \mathcal{Y}^l \mathcal{W}(\mathcal{Y})$ and the scaled transition rate $\mathcal{W}(\mathcal{Y})$ can be represented by an integral transform of $\phi(v)$ for the cylindrically symmetric case:

$$\Phi(s) = -\frac{2\rho h w v_0}{\tilde{s}^2 \tilde{w}^2} \int_0^{\infty} dx \tilde{\phi}(x) \{ -(\tilde{w} \tilde{s} x) \pi H_0(\tilde{w} \tilde{s} x) + 2(\tilde{w} \tilde{s} x)^2 \}. \quad (4)$$

Here, we have introduced dimensionless variables $\tilde{w} = (1 + e)w/2R_I$, $\tilde{s} = s v_0/R_I$, $x = v/v_0$, and $\tilde{\phi}(x) = v_0^2 \phi(v_0 x)$. We have used the Struve function $H_\nu(x)$ with $\nu = 0$ defined by Eq. (B6) [82]. See Appendix B for the detailed derivation. We note that Eq. (4) is valid not only for the linear (viscous) frictional rotor but also for the nonlinear (dry) frictional rotor. Substituting Eq. (4) into Eq. (3), we obtain

$$\frac{\tilde{\gamma}}{\pi k} \left\{ k^3 \frac{d}{dk} \ln \tilde{P}_{\text{ss}} \left(\frac{k}{\tilde{w}} \right) + B k^2 \right\} = \int_0^{\infty} dx x \tilde{\phi}(x) H_0(kx), \quad (5)$$

where we have introduced $B = (2/\tilde{\gamma}) \int_0^{\infty} dx x^2 \tilde{\phi}(x)$, a dimensionless variable $k \equiv \tilde{w} \tilde{s}$, and a scaled friction coefficient $\tilde{\gamma} \equiv \gamma/(2\rho h w I v_0)$. The integral on the right hand side of Eq. (5) is known as the Struve transformation, and its inverse transformation is the Y transform, which are kinds of the Bessel transformations [83]. Introducing the Neumann function $N_\nu(x)$ with $\nu = 0$ [82], we obtain the inverse estimation formula:

$$\tilde{\phi}(x) = \int_0^{\infty} G_{\text{vis}}(k) N_0(kx) k dk, \quad (6)$$

$$G_{\text{vis}}(k) \equiv \frac{\tilde{\gamma}}{\pi k} \left\{ k^3 \frac{d}{dk} \ln \tilde{P}_{\text{ss}} \left(\frac{k}{\tilde{w}} \right) + B k^2 \right\}. \quad (7)$$

The VDF of the granular gas can be determined from Eqs. (6) and (7) only through the observation of the rotor dynamics. This implies that the rotor is regarded as a thermometer for the granular gas with the aid of the inverse formula Eqs. (6) and (7). The constant B in Eq. (7) can be determined numerically by the condition $\lim_{k \rightarrow \infty} G_{\text{vis}}(k) = 0$.

B. Forward problem for viscous rotor

Before considering the inverse problem, we discuss the forward problem, i.e., the determination of the PDF for the rotor from the VDF for the granular gas. We verify the validity of the formulas (3) and (4) using the numerical data of the VDF $\phi(v)$ for the granular gas under gravity. In the following numerical simulation, we adopt $\gamma/mL_{\text{box}}v_0 = 2.0$, which corresponds to $\tilde{\gamma} = 1.15248$. In Fig. 4 (a), we plot $P_{\text{ss}}(\Omega)$ by the solid line on the basis of Eqs. (3) and (4) and the numerical data for $\phi(v)$ and the results of the MD simulation (circles). The agreement between the theory and the simulation is good except for the point near $\Omega = 0$, where the numerical error would be decreased by smaller bin-width for $\phi(v)$. We adopt the bin-width of the numerical histogram for $\phi(v)$ as $5.0 \times 10^{-3} v_0$. See Appendix C 1 for the detailed procedure to obtain the solid line in Fig 4 (a).

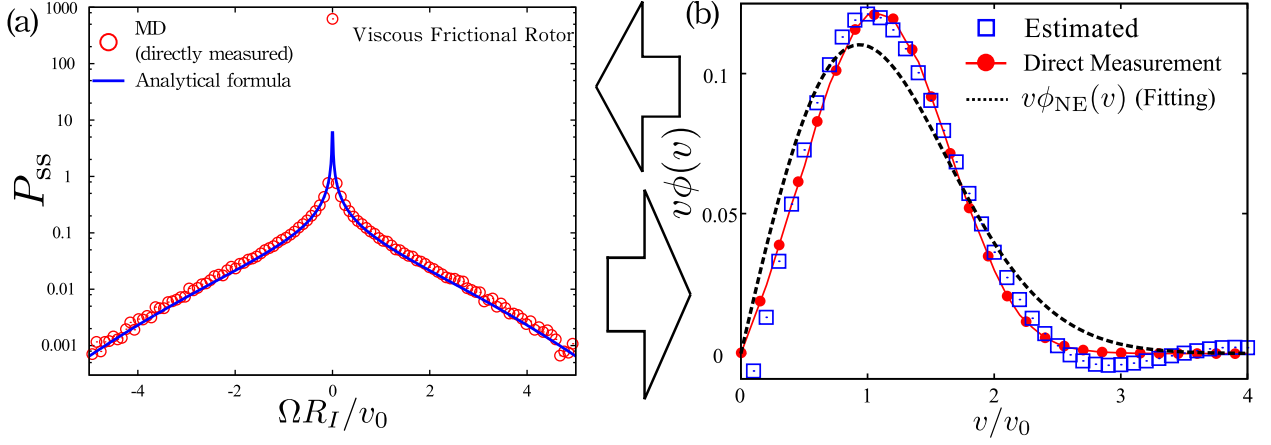


FIG. 4: (Color online) The demonstration of the applicability of our formulas (3)-(7) under viscous friction on (a) the forward and (b) the inverse estimation problems. The Fourier transform of Eq. (3) is shown as the solid line (a), which agrees with the directly measured MD data. (b) Our formula (6) represented by open squares are compared with the numerical data for the VDF $\phi(v)$ near the rotor (filled circles). We can successfully estimate the VDF for the granular gas only observing the angular VDF for the rotor. Note that there exists the numerical error for large v/v_0 .

C. Inverse problem for granular gas

In this subsection, we show that the VDF for the granular gas can be inferred only through the numerical data of a steady distribution for the angular velocity of a frictional rotor by using the formula Eq. (6) associated with Eq. (7).

The result for the inverse formula in Eqs. (6) and (7) is shown in Fig. 4 (b), where the parameter B is estimated as $B = 0.365556$ and we have used the bin-width $8.660211 \times 10^{-5} v_0 / R_I$ for P_{ss} . The dotted line is $v\phi_{NE}(v)$, and our formula (6) represented by open squares correctly predicts the numerical data for the VDF $\phi(v)$ near the rotor (filled circles). We adopt the bin-width for P_{ss} as $8.660211 \times 10^{-5} v_0 / R_I$. Although numerical oscillation exists for large v/v_0 , our estimation for the granular bath based on Eq. (6) agrees well with the directly measured VDF of granular particles in the MD simulation. This implies that the inverse formula (6) supplemented by Eq. (7) enables us to use the motion of the rotor as a non-equilibrium thermometer. See Appendix C 2 for the detailed procedure to obtain the estimated VDF.

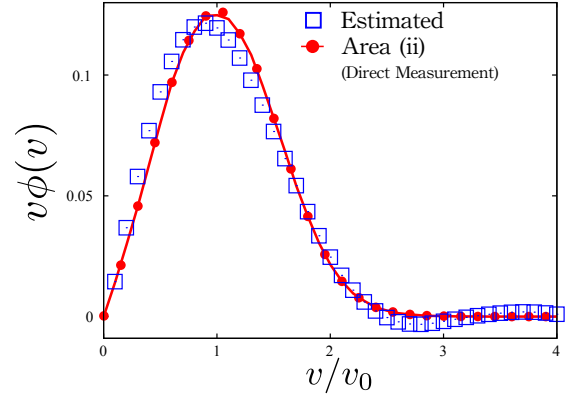


FIG. 5: (Color online) The demonstration of the inverse formula for the local VDF in the area (ii). Although the accuracy is a little worse than that in Fig. 4, the estimated data (squares) correctly predicts the direct measurement data (circles).

V. POSITION DEPENDENCE OF THE ROTOR

We now discuss the utility of the rotor as a local non-equilibrium probe. In Sec. IV C, we have already demonstrated that the VDF for the surrounding gas in the area (i) can be inferred from the angular VDF for the viscous rotor P_{ss} . Here, we discuss whether we can infer the local VDF in the area (ii) from the motion of the rotor using Eqs. (6) and (7).

In Fig. 5, we show that the VDF in the area (ii) can be also inferred from the angular VDF of the rotor. The

estimated data and the directly measured data are represented by squares and circles, respectively. See also Appendix C 2 for the detailed procedure to obtain the estimated $\phi(v)$. Here, the parameter B is estimated as $B = 0.40278$. There also exists the numerical oscillation for large v/v_0 . Although the accuracy is not as good as Fig. 4 (b), the estimated data are consistent with those obtained by the direct measurement. The reason for the small discrepancy would be the violation of the cylindrical symmetry because of the influence of the wall.

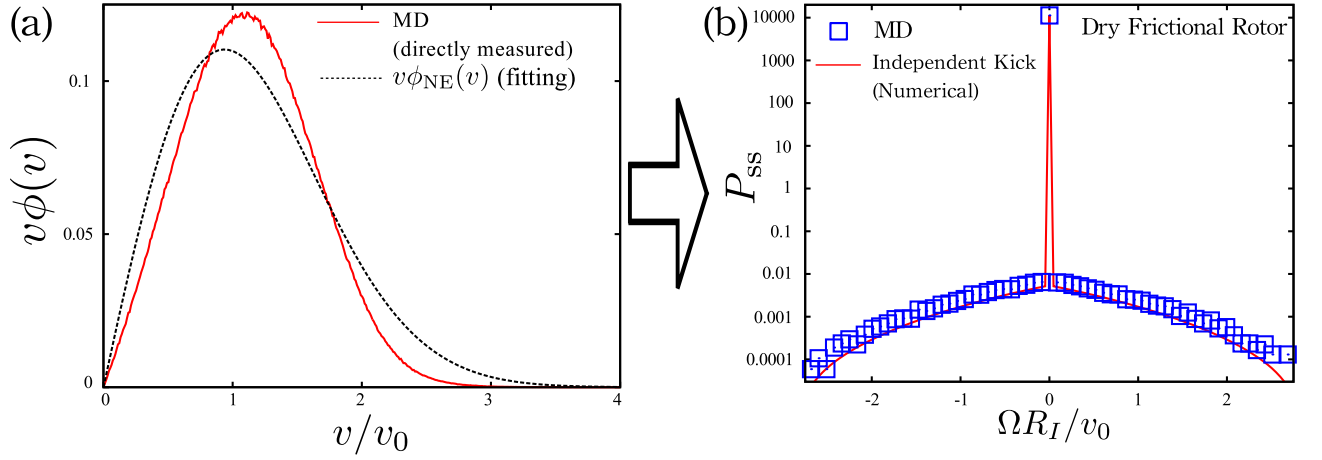


FIG. 6: (Color online) $P_{ss}(\Omega)$ for the dry frictional rotor is calculated using the VDF represented (the solid line in (a)). The steady state angular VDF for the dry frictional rotor is shown in (b). The squares and the solid line are histogram for MD and the Fourier transform of Eq. (8), respectively. Our observed histogram in MD simulation can be correctly predicted by the Fourier transform of Eq. (8)

VI. GRANULAR ROTOR UNDER DRY FRICTION

We, now, consider a rotor under dry friction $N_{fri} = -\Delta \text{sgn}(\omega)$, because real experimental rotors are influenced by dry friction [57–59]. In Sec. VIA, we derive an analytic formula for the angular VDF of the rotor, and verify its validity in Sec. VIB. Note that we here only study the forward problem on the basis of the perturbative method developed in Ref. [47, 49].

A. Analytic formula for PDF of the rotor

The steady angular VDF $P_{ss}(\Omega)$ can be obtained perturbatively in terms of $1/\tilde{\Delta}'$ with $\tilde{\Delta}' \equiv \Delta(1 + e)/(\epsilon I \rho h v_0^2 4\pi) \gg 1$. The first-order solution in terms of $1/\tilde{\Delta}'$ is known as the independent kick model, which is originally introduced in Ref. [49] and can be systematically derived in Refs. [46, 47]. Introducing the Bessel function $J_\nu(x)$ [82], \tilde{P}_{ss} for the rotor under the dry friction can be rewritten as:

$$\tilde{P}_{ss}\left(\frac{k}{\tilde{w}}\right) = 1 + \frac{\tilde{w}^2}{k^2} \frac{1}{\tilde{\Delta}'} \left[\frac{1}{2\pi} + C_1 k^2 - G_{\text{dry}}(k) \right] + O(1/\tilde{\Delta}'^2), \quad (8)$$

$$G_{\text{dry}}(k) \equiv \int_0^\infty dx x \tilde{\phi}(x) J_0(kx), \quad (9)$$

where we have introduced $C_1 = -\int_0^\infty dx x^3 \tilde{\phi}(x)/4$. See Appendix D for the detailed derivation.

B. Forward problem for dry frictional rotor

Now, let us examine whether Eqs. (8) and (9) are consistent with the result of MD. For the MD simulation, we adopt $\Delta/mv_0^2 = 20.0$, which corresponds to $\tilde{\Delta}' = 31.36531$. The bin-width for P_{ss} is set to be $8.660211 \times 10^{-5} v_0/R_I$. As shown in Fig. 6 (b), the obtained PDF $P_{ss}(\Omega)$ in the MD simulation is correctly predicted by the Fourier transform of Eq. (8) using the numerical data of VDF for the granular gas $\phi(v)$ (Fig. 6 (a)). We have also checked that the VDF for the granular gas is invariant even if we change the frictional torque N_{fri} of the rotor. We stress that the VDF of the granular gas obtained in MD cannot be fitted by that activated by the white noise thermostat [25]. In Fig. 6 (b), the squares and the solid line are histograms for MD and the Fourier transform of Eq. (8), respectively. For a given VDF of the granular gas, our framework agrees with the results of the MD simulation without introducing any fitting parameters. It should be noted that one can find the small discrepancy between the theoretical result and the data for large $\Omega R_I/v_0$, because the independent kick model is correct only for small $\Omega R_I/v_0$. See the detailed implementation of Eqs. (8) and (9) in Appendix. E.

We here discuss the difficulty for the inverse estimation problem under dry friction in the present theoretical analysis. A possible reason is as follows: Although Eq. (8) can be formally solved in terms of $\tilde{\phi}$, the formal inverse formula is practically useless because the independent kick model under dry friction is only valid for small $\Omega R_I/v_0$ and the inverse Fourier transformation of Eq. (8) does not work well. Indeed, the exponential tail is reported for the dry frictional rotor for large $\Omega R_I/v_0$ in Ref. [47], which cannot be captured by the independent kick solution.

VII. SUMMARY AND DISCUSSION

We have examined the role of a granular rotor as a local non-equilibrium probe through the MD simulation of the rotor in vibrating granular beds under gravity (Figs. 1 and 2). We have approximately observed the cylindrically symmetric and spatially inhomogeneous VDFs (Fig. 3). We have formulated the inverse formula (6) in cylindrical coordinates to apply the MD simulation of a realistic viscous rotor. Starting from the Boltzmann-Lorentz equation (1), we have derived an analytic result Eq. (6) supplemented by Eq. (7) for the viscous frictional rotor. Using Eq. (6), we have numerically calculated the angular VDF for the rotor from the data of VDF for the granular gas near the rotor, and vice versa in Fig. 4. Furthermore, we have demonstrated that our inverse formula can be used even if the location of the rotor is different from the center of the container as shown in Fig. 5. Thus, the granular rotor is useful as a local probe for non-equilibrium baths.

For a dry frictional rotor, we have considered only the forward problem, and the result agrees with the MD result, as shown in Fig. 6. In other words, we cannot solve the inverse problem for the dry frictional rotor. To derive an alternative valid inverse formula for the dry frictional rotor, we expect that an appropriate interpolation is necessary between Eq. (8) and the exponential tail of the VDF for the rotor

Let us discuss the possible extension of our work. We have assumed the restitution coefficient of grains is constant [61, 62]. The restitution coefficient for a sphere depends on the impact velocity v_{imp} as $e(v_{\text{imp}}) = 1 - \mathcal{B}_1 v_{\text{imp}}^{1/5} + \dots$ ($\mathcal{B}_1 > 0$) [14, 84]. As discussed in Ref. [85], the velocity dependence of the restitution coefficient is introduced to the Boltzmann-Lorentz equation, which can be also analyzed in our theory in a similar manner. The effects for the tangential interaction and the mutual rotation between grains are also necessary to be analyzed. The extension of the Boltzmann equation toward denser gas is known as the Enskog equation [26, 27]. It would be possible and interesting to apply our framework to the rotor in dense granular media [86] or denser granular liquids near the jamming transition beyond Enskog equation [39], by modifying the transition probability W_ϵ in Eq. (1) [87]. As a future problem, it is also necessary to estimate the amount of the errors in particular for the inverse estimation formulas Eqs. (6) and (7).

Acknowledgement

We are grateful for useful discussion with A. Puglisi and A. Gnoli. The numerical calculations were carried out on SR16000 at YITP in Kyoto University. This work is supported by the Grants-in-Aid for Japan Society for Promotion of Science (JSPS) Fellows (Grants No. 26-2906 and No.27-6208), and JSPS KAKENHI (Grant

No. 25287098). This work is also partially supported by the JSPS core-to-core program for Nonequilibrium dynamics for soft matter and information.

Appendix A: Benchmark Test for Simulation

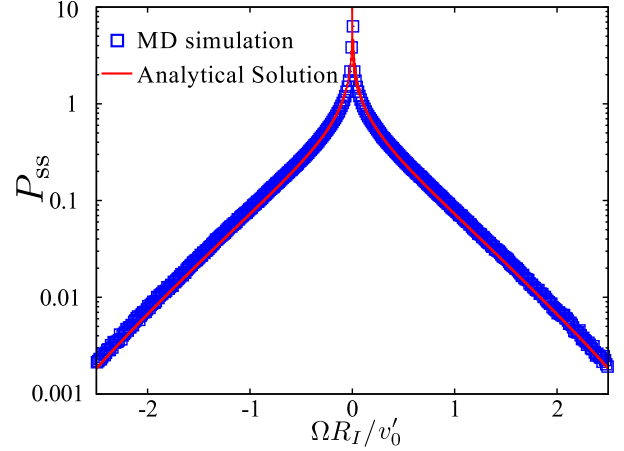


FIG. 7: (Color online) The results of MD simulation under viscous friction (squares) and our analytical solution are compared. The solid line represents the Fourier transform of Eq. (A1). Our exact solution perfectly agrees with the MD simulation data.

In this appendix, we show that P_{ss} observed in our MD simulation can be analytically predicted when the gas is elastic ($e_g = e = 1$) without gravity $g = 0$ and vibration, fixing $z_{\text{max}} = 0$ as a benchmark test. We analyze a container heated by the thermal wall at the bottom. The top and the side walls of the container are chosen to be smooth elastic walls. The thermal wall is chosen to be the diffusive wall, i.e., the post collisional velocity of a grain $\mathbf{v} = (v_x, v_y, v_z)$ against the thermal wall is chosen to be random, following the distribution $\phi_{\text{wall}}(\mathbf{v}, T_{\text{bath}}) = (m/T_{\text{wall}})^2 v_z \exp[-m\mathbf{v}^2/2T_{\text{wall}}] / 2\pi$ [67, 68]. We choose the typical velocity in this setup $v'_0 = \sqrt{T_{\text{wall}}/m}$ instead of v_0 as in Sec. II. We have numerically checked that the VDF for the elastic gas can be regarded as the Gaussian $\tilde{\phi}(x) = \phi_G(x)$ with $x = v/v'_0$. P_{ss} can be obtained analytically from our theory. The obtained solution is compared with the MD simulation data in Fig. 7 for the viscous rotor.

With the aid of Eqs. (3) and (4), we obtain the analytic solution for $P_{ss}(\Omega)$ as

$$\tilde{P}_{ss}\left(\frac{k}{\tilde{w}}\right) = \exp\left[-\frac{1}{3\tilde{\gamma}\sqrt{2\pi}}\frac{k^2}{2}{}_2F_2\left(\frac{1, 1}{2, \frac{5}{2}}\middle|-\frac{k^2}{2}\right)\right], \quad (\text{A1})$$

where we have used the following formulas $\tilde{\gamma}B = 1/\sqrt{2\pi}$,

$\pi k \int_0^\infty dx x \phi_G(x) H_0(kx) = k D_F(k/\sqrt{2})/\sqrt{\pi}$, and

$$\int_0^{\frac{k}{\sqrt{2}}} \frac{ds'}{s'} \left(\frac{D_F(s')}{s'} - 1 \right) = -\frac{k^2}{6} {}_2F_2 \left(\begin{matrix} 1, 1 \\ 2, \frac{5}{2} \end{matrix} \middle| -\frac{k^2}{2} \right). \quad (\text{A2})$$

Here, $D_F(x)$ is the Dawson function [82]:

$$D_F(x) \equiv e^{-x^2} \int_0^x e^{t^2} dt \quad (\text{A3})$$

and ${}_qF_p$ is the generalized hypergeometric function [82, 89]:

$${}_qF_p \left(\begin{matrix} a_1, a_2, \dots, a_q \\ b_1, b_2, \dots, b_p \end{matrix} \middle| z \right) \equiv \sum_{l=0}^{\infty} \frac{(a_1)_l (a_2)_l \dots (a_q)_l}{(b_1)_l (b_2)_l \dots (b_p)_l} \frac{z^l}{l!}, \quad (\text{A4})$$

where we have introduced the Pochhammer symbol as $(a)_l \equiv \Gamma(a+l)/\Gamma(a)$ with $l \geq 0$. To plot Fig. 7, we adopt $\gamma/mL_{\text{box}}v_0 = 1.0$, which corresponds to $\tilde{\gamma} = 0.57624$. The histogram for the angular velocity is shown in Fig. 7 and the analytical solution (solid line) is consistent with the MD simulation result (squares), which ensures the accuracy of our MD code and the validity of our framework.

Appendix B: Detailed derivation of the formulas for a viscous frictional rotor

In this appendix, we show the detailed derivation of the analytic results for the viscous frictional rotor in Sec. IV. Introducing $\mathcal{Y} \equiv y/\epsilon$, the transition rate given by $\mathcal{W}(\mathcal{Y}) \equiv \tilde{W}(\omega = 0; \mathcal{Y})$ is independent of ϵ and Ω . We note that $W_\epsilon(\omega; y)$ satisfies the relation $\tilde{W}(\omega; \mathcal{Y}) d\mathcal{Y} = W_\epsilon(\omega; y) dy$ up to the leading order. We obtain the reduced time evolution equation for $\mathcal{P} = \mathcal{P}(\Omega, t)$ in $\epsilon \rightarrow 0$ limit from Eq. (1) when the axial friction is sufficiently strong, according to the generalized system size expansion method [46, 47]. For general frictional torque $N_{\text{fri}} = N_{\text{fri}}(\omega)$, we obtain

$$\begin{aligned} \frac{\partial \mathcal{P}}{\partial t} &= -\frac{1}{I} \left\{ \frac{\partial}{\partial \Omega} \tilde{N}_{\text{fri}}(\Omega) \mathcal{P} \right\} \\ &+ \int_{-\infty}^{\infty} d\mathcal{Y} \mathcal{W}(\mathcal{Y}) \{ \mathcal{P}(\Omega - \mathcal{Y}, t) - \mathcal{P}(\Omega, t) \}, \end{aligned} \quad (\text{B1})$$

$$\begin{aligned} \mathcal{W}(\mathcal{Y}) &= \rho h \int_0^{2w} d\varrho \int_{-\infty}^{\infty} dv_x dv_y \phi(v_x, v_y) \Theta(-v_n) \\ &\times | -v_n | \delta(\mathcal{Y} - \Delta\bar{\omega}'), \end{aligned} \quad (\text{B2})$$

$$\Delta\bar{\omega}' \equiv -\frac{1+e}{R_I} g(\varrho) v_n, \quad (\text{B3})$$

where we have introduced the rescaled friction $\tilde{N}_{\text{fri}}(\Omega) = N_{\text{fri}}(\epsilon\Omega)/\epsilon$. It should be noted that $\tilde{N}_{\text{fri}}(\Omega) = O(1)$ is assumed in $\epsilon \rightarrow 0$ limit.

The scaled friction is written as $\tilde{N}_{\text{fri}} = -\tilde{\gamma}\Omega$ in Eq. (B1) for the case of viscous friction with $\tilde{\gamma} =$

$\gamma/(2\rho h w I v_0)$. We calculate the cumulant generating function $\Phi(s)$. For an even integer l , the cumulant $\mathcal{K}_l = \int d\mathcal{Y} \mathcal{Y}^l \mathcal{W}(\mathcal{Y})$ is calculated as

$$\begin{aligned} \mathcal{K}_l &= \rho h \int_0^{2w} d\varrho \int_{-\infty}^{\infty} dv_x dv_y \phi(v_x, v_y) \\ &\times \Theta(-v_n) | -v_n | (\Delta\bar{\omega}')^l \\ &= \rho h \frac{(1+e)^l}{R_I^l} 2 \int_{-w/2}^{w/2} d\varrho' \left(\frac{\varrho'}{R_I} \right)^l \\ &\times \int_0^\infty dv v \int_0^{2\pi} d\theta \phi(v) \Theta(-v \cos \theta) (-v \cos \theta)^{l+1} \\ &= \rho h \frac{(1+e)^l}{R_I^l} 4 \int_0^{w/2} d\varrho' \left(\frac{\varrho'}{R_I} \right)^l \\ &\times \int_0^\infty dv v^{l+2} \phi(v) \frac{\Gamma(\frac{l+2}{2})}{\Gamma(\frac{l+3}{2})} \sqrt{\pi} \\ &= \rho h \frac{\sqrt{\pi}(1+e)^l}{R_I^{2l}} \frac{\Gamma(\frac{l+2}{2})}{\Gamma(\frac{l+3}{2})} \\ &\times \frac{4}{l+1} \left(\frac{w}{2} \right)^{l+1} \int_0^\infty dv v^{l+2} \phi(v). \end{aligned} \quad (\text{B4})$$

We have changed the coordinate variable ϱ to ϱ' satisfying $-w/2 < \varrho' < w/2$, and used the front-back symmetry for the rotor. Here, $\Gamma(y)$ represents the Gamma function $\Gamma(y) = \int_0^\infty s^{y-1} e^{-s} ds$. Then, $\Phi(s)$ is written as

$$\begin{aligned} \Phi(s) &= \int_0^\infty dv \phi(v) 2\sqrt{\pi} \rho h \sum_{l=1}^\infty \frac{w^{l+1} v^{l+2}}{R_I^{2l} 2^l} \\ &\times \frac{(is)^l (1+e)^l}{(l+1)!} \frac{\Gamma(\frac{l+2}{2})}{\Gamma(\frac{l+3}{2})} \\ &= -\int_0^\infty dv \phi(v) 2\sqrt{\pi} \rho h w \frac{R_I^4}{w^2 s^2} \left(\frac{2}{1+e} \right)^2 \\ &\times \left\{ \sum_{j=2}^\infty \frac{(-1)^j}{(2j-1)!} \frac{\Gamma(j)}{\Gamma(j+\frac{1}{2})} \left(\frac{1+e}{2} \frac{w s v}{R_I^2} \right)^{2j} \right\} \\ &= -\int_0^\infty d\tilde{v} \tilde{\phi}(\tilde{v}) \frac{2\rho h w v_0}{\tilde{s}^2 \tilde{w}^2} \\ &\times \{ -(\tilde{w} \tilde{s} \tilde{v}) \pi H_0(\tilde{w} \tilde{s} \tilde{v}) + 2(\tilde{w} \tilde{s} \tilde{v})^2 \}, \end{aligned} \quad (\text{B5})$$

where we have introduced the Struve function

$$H_0(y) = \sum_{l=0}^\infty \frac{(-1)^l y^{2l+1}}{\{(2l+1)!!\}^2}. \quad (\text{B6})$$

Because $\Phi(s)$ and \tilde{P}_{ss} satisfy the relation

$$\Phi(s) = s \frac{\gamma}{I} \frac{d}{ds} \ln \tilde{P}_{\text{ss}}, \quad (\text{B7})$$

we obtain

$$\begin{aligned} \tilde{s}^3 \frac{d}{d\tilde{s}} \ln \tilde{P}_{\text{ss}} &= \frac{2\rho h w I v_0}{\gamma \tilde{w}^2} \int_0^\infty d\tilde{v} \tilde{\phi}(\tilde{v}) \\ &\times \{ (\tilde{w} \tilde{s} \tilde{v}) \pi H_0(\tilde{w} \tilde{s} \tilde{v}) - 2(\tilde{w} \tilde{s} \tilde{v})^2 \}. \end{aligned} \quad (\text{B8})$$

Introducing variables $k = \tilde{w}\tilde{s}$ and $x = \tilde{v}$, we obtain

$$\tilde{\gamma} \left\{ k^3 \frac{d}{dk} \ln \tilde{P}_{ss} \left(\frac{k}{\tilde{w}} \right) + Bk^2 \right\} = \pi k \int_0^\infty dx x \tilde{\phi}(x) H_0(kx), \quad (\text{B9})$$

where we have introduced $B = (2/\tilde{\gamma}) \int_0^\infty dx x^2 \tilde{\phi}(x)$. Thus, we obtain the formula (5).

Appendix C: Detailed procedure to apply the formula Eqs. (6) and (7)

1. Forward problem

Let us explain the detailed numerical technique to obtain $P_{ss}(\Omega)$ using Eqs. (3) and (4). It contains the following four steps (a)-(d):

(a) Measure the VDF for the granular gas $\tilde{\phi}(x)$ around the rotor.

(b) Obtain the extrapolated data for $x\tilde{\phi}(x)$ in $x \rightarrow \infty$ limit. We fit the data in the range $x_- < x < x_+$ by a function $b_1 \exp(-b_2 x)$. We replace the data for $x > x_{\text{cut}}$ and extrapolate the data by the fitting function in $x < x_{\text{end}}$. We have checked whether the results are invariant if we use Gaussian as a fitting function instead.

(c) Apply the Struve transform in Eq. (4) using Eq. (B6).

(d) Obtain the Fourier transform $\tilde{P}_{ss}(s)$. Note that $P_{ss}(\Omega)$ has a sharp peak around $\Omega = 0$, which is serious for the numerical Fourier transformation in terms of convergence. To solve this problem, we use the double exponential formula, which is a numerical technique for singular functions [88].

In Sec. IV B, we adopt the fitting ranges as $x_- = x_{\text{cut}} = 3.0$, $x_+ = 5.0$, and $x_{\text{end}} = 60.0$, and obtained fitting parameters are $b_1 = 5910.96$ and $b_2 = 5.64439$.

2. Inverse estimation problem

Let us explain the detailed numerical technique to obtain $\phi(v)$ on the basis of Eqs. (6) and (7). It contains the following seven steps (a)-(g), to obtain $\tilde{\phi}$ from the data of $P_{ss}(\Omega)$.

(a) Obtain the data of $P_{ss}(\Omega)$.

(b) Obtain the extrapolated data of $P_{ss}(\Omega)$ for $\Omega \rightarrow \infty$. We fit the data in the range $\Omega_- < \Omega < \Omega_+$ by the function $b'_1 \exp(-b'_2 \Omega)$. Replace the data for $\Omega > \Omega_{\text{cut}}$ and extrapolate the data $\Omega < \Omega_{\text{end}}$ by the fitting function. We have also checked that the results are invariant if we use the Gaussian fitting function instead.

(c) Obtain the Fourier transform $\tilde{P}_{ss}(s)$. We have applied the double exponential formula [88], similarly to the forward problem.

(d) Estimate the parameter B . Fit the data of $k^3 d \log \tilde{P}/dk$ for $k \rightarrow \infty$ by the function $c' - Bk^2$. In our analysis, we fit the data in the region $k_e^- < k < k_e^+$.

(e) Calculate $G_{\text{vis}}(k)$ using Eq. (7).

(f) Fit the numerically obtained data of $G_{\text{vis}}(k)$ in the procedure (e) by $c/k + d/k^3$ in the $k \rightarrow \infty$ limit. In our analysis, we fit the data in the region $k_e^- < k < k_e^+$, and replace and extrapolate the data for $k'_{\text{cut}} < k < k'_{\text{end}}$ by the fitting function, where the cutoffs satisfy $k_e^- < k'_{\text{cut}} < k_e^+$.

(g) Apply the Y transform (6) using the data of $G_{\text{vis}}(k)$ obtained in the procedure (e).

Fitting ranges used in Sec. IV C are listed as $\Omega_- = 4.0v_0/R_I$, $\Omega_+ = 5.0v_0/R_I$, $\Omega_{\text{cut}} = 4.0v_0/R_I$, $\Omega_{\text{end}} = 20.0\Omega_{\text{cut}}$, $k_e^- = 3.0$, $k_e^+ = 5.0$, $k_e^- = 2.5$, $k_e^+ = 3.5d = 0.603414$, $k'_{\text{cut}} = 3.0$, and $k'_{\text{end}} = 5.968133 \times 10^4$, and obtained fitting parameters are $b'_1 = 0.438068R_I/v_0$, $b'_2 = 1.26993R_I/v_0$, $c' = 0.40721$, and $c = 0.0942702$.

In Sec. V, fitting ranges and parameters are listed as $\Omega_- = 4.0v_0/R_I$, $\Omega_+ = 5.0v_0/R_I$, $b'_1 = 0.463788R_I/v_0$, $b'_2 = 1.31134R_I/v_0$, $\Omega_{\text{cut}} = 4.0v_0/R_I$, $\Omega_{\text{end}} = 20.0\Omega_{\text{cut}}$, $k_e^- = 3.0$, $k_e^+ = 5.0$, $c' = 0.660408$, $k_e^- = 2.5$, $k_e^+ = 3.5$, $c = 0.169773$, $d = 0.557026$, $k'_{\text{cut}} = 3.0$, and $k'_{\text{end}} = 5.968133 \times 10^4$.

Appendix D: Detailed derivation of the formulas for a dry frictional rotor

In this appendix, we show the detailed derivation of the analytical results for the dry frictional rotor in Sec. VI. The scaled dry friction in Eq. (B1) is written as $\tilde{N}_{\text{fri}}(\Omega) = -\tilde{\Delta} \text{sgn}(\Omega)$, where we have introduced $\tilde{\Delta} \equiv \Delta/\epsilon$. The independent kick solution is written as

$$\tilde{P}_{ss}(s) = 1 + \frac{I}{\tilde{\Delta}} \int_{-\infty}^{\infty} d\mathcal{Y} \mathcal{W}(\mathcal{Y}) \int_0^{\mathcal{Y}} \frac{d\Omega}{\text{sgn}(\Omega)} [e^{is\Omega} - 1] + O(1/\tilde{\Delta}'^2). \quad (\text{D1})$$

Equation (D1) is rewritten as

$$\begin{aligned} \frac{\tilde{\Delta}}{I} (\tilde{P}_{ss} - 1) &= \int_{-\infty}^{\infty} d\mathcal{Y} \mathcal{W}(\mathcal{Y}) \int_0^{\mathcal{Y}} \frac{d\Omega}{\text{sgn}(\Omega)} \sum_{l=1}^{\infty} \frac{(is\Omega)^l}{l!} \\ &= \sum_{l=1}^{\infty} \frac{(is)^l}{l!} \int_{-\infty}^{\infty} d\mathcal{Y} \mathcal{W}(\mathcal{Y}) \frac{\text{sgn}(\mathcal{Y}) \mathcal{Y}^{l+1}}{l+1} \\ &= \sum_{j=1}^{\infty} \frac{(-1)^j s^{2j+2}}{(2j+1)!} \int_{-\infty}^{\infty} d\mathcal{Y} |\mathcal{Y}|^{2j} \mathcal{W}(\mathcal{Y}) \frac{1}{s^2}. \end{aligned} \quad (\text{D2})$$

By noting the following relations for an even integer l :

$$\begin{aligned}
\int_{-\infty}^{\infty} d\mathcal{Y} |\mathcal{Y}| \mathcal{Y}^l \mathcal{W}(\mathcal{Y}) &= \frac{4\rho h(1+e)^{l+1}}{R_I^{2l+2}(l+2)} \left(\frac{w}{2}\right)^{l+2} \\
&\times \int_0^{\infty} dv v^{l+3} \phi(v) \\
&\times \int_{-\pi/2}^{\pi/2} d\theta \cos^{l+2} \theta \\
&= \frac{4\rho h(1+e)^{l+1} \sqrt{\pi}}{R_I^{2l+2}(l+2)} \left(\frac{w}{2}\right)^{l+2} \frac{l+4}{l+3} \\
&\times \frac{(\frac{l}{2} + \frac{3}{2})!}{(\frac{l}{2} + 2)!} \int_0^{\infty} dv v^{l+3} \phi(v),
\end{aligned} \tag{D3}$$

$$\begin{aligned}
\int_{-\pi/2}^{\pi/2} d\theta \cos^{l+2} \theta &= \sqrt{\pi} \frac{\Gamma(\frac{l+3}{2})}{\Gamma(\frac{l+4}{2})} \\
&= \frac{l+4}{l+3} \frac{(\frac{l}{2} + \frac{3}{2})!}{(\frac{l}{2} + 2)!},
\end{aligned} \tag{D4}$$

$$\frac{(2j+4)(j+\frac{3}{2})!}{(2j+3)!(j+2)!} = \sqrt{\pi} \left(\frac{1}{2^{j+1}(j+1)!} \right)^2, \tag{D5}$$

$$J_0(x) = 1 - \sum_{j=0}^{\infty} \frac{(-1)^j x^{2(j+1)}}{2^{2(j+1)} \{(j+1)!\}^2} \tag{D6}$$

we obtain

$$\begin{aligned}
\frac{\tilde{\Delta}}{I} \left\{ \tilde{P}_{ss} \left(\frac{k}{\tilde{w}} \right) - 1 \right\} \left(\frac{k}{\tilde{w}} \right)^2 &= \frac{4\pi\rho h v_0^2}{1+e} \int_0^{\infty} dx x \tilde{\phi}(x) \\
&\times \left\{ 1 - \frac{k^2 x^2}{4} - J_0(kx) \right\}.
\end{aligned} \tag{D7}$$

We introduce coefficients here for Appendix E:

$$C_l \equiv \frac{(-1)^l}{2^{2l}(l!)^2} \int_0^{\infty} dx x^{2l+1} \tilde{\phi}(x), \tag{D8}$$

with a positive integer $l = 1, 2, \dots$. We thus obtain Eq. (8) and (9) from Eq. (D7).

Appendix E: Detailed procedure to apply the formula Eqs. (8) and (9)

We, here, explain the detailed techniques to use the analytic PDF formulas (8) and (9). There are the following six steps (a)-(f) to obtain $P_{ss}(\Omega)$ numerically.

(a) Observe the granular velocity around the rotor and make a histogram to numerically obtain the VDF $\tilde{\phi}(x)$.

(b) Introducing the sufficiently large x_- and x_+ ($x_- < x_+$), obtain the extrapolated data for $x\tilde{\phi}(x)$ in the $x \rightarrow \infty$ limit. We fit the data in the range $x_- < x < x_+$ by the exponential function $b_1 \exp(-b_2 x)$. We replace the data for $x > x_{\text{cut}}$ and extrapolate the data by $x < x_{\text{end}}$ by the fitting function. We have also checked that the results are invariant if we use Gaussian as a fitting function instead.

(c) Obtain $G_{\text{dry}}(k)$ as the Bessel transform of $\tilde{\phi}$ Eq. (9), and calculate C_1 and C_2 according to Eq. (D8).

(d) Replace the data of $G_{\text{dry}}(k)$ for $k < k_{\text{cut}}^-$ by $1/2\pi + C_1 k^2 + C_2 k^4$, which corresponds to the Taylor expansion of Eq. (9) to avoid the numerical divergence of the second term in Eq. (8) in the $k \rightarrow 0$ limit. In the range $k_d^- < k < k_d^+$, fit the data of $G_{\text{dry}}(k)$ by $d_1 \exp(-d_2 k^2)$. We extrapolate the data by $d_1 \exp(-d_2 k^2)$ in the region $k > k_{\text{cut}}^+$.

(e) Calculate $P_{\text{inf}} \equiv \lim_{s \rightarrow \infty} \tilde{P}_{ss}(s) = 1 + C_1 \tilde{w}^2 / \tilde{\Delta}'$, which corresponds to the delta function for $P_{ss}(\Omega)$, and obtain the data for $\tilde{P}_{ss}(s)$, following Eq. (8).

(f) Apply the Fourier transform to the data for $P_{ss}(s) - P_{\text{inf}}$, and obtain the smooth part $P_{ss}^{\text{smooth}}(\Omega)$. We note $P_{ss}(\Omega = 0) = P_{ss}^{\text{smooth}}(0) + P_{\text{inf}}/\Delta\Omega$. Here, $\Delta\Omega$ is the data mesh for Ω . Finally we obtain $P_{ss}(\Omega) = P_{\text{inf}}\delta(\Omega) + P_{ss}^{\text{smooth}}(\Omega)$.

We extrapolate the data in the procedure (b) and (d), because a large number of data are necessary to numerically perform integral transforms twice, in the Fourier and Bessel transform (8) and (9). The data are extrapolated also in Sec. IV C, for the same reason.

In Sec. VI, we adopt the fitting ranges as $x_- = 3.0$, $x_+ = 5.0$, $x_{\text{end}} = 20.0x_-$, $x_{\text{cut}} = x_-$, $k_{\text{cut}}^- = 0.5$, $k_d^- = 1.5$, $k_d^+ = 2.0$, and $k_{\text{cut}}^+ = 1.75$, and obtained fitting parameters are $b_1 = 5910.96$, $b_2 = 5.64439$, $d_1 = 0.204485$, and $d_2 = 0.527407$.

-
- [1] L. Landau and E. Lifshitz, *Statistical Physics, Part 1* (Butterworth-Heinemann, Oxford, 1980).
 - [2] H. Callen, *Thermodynamics and an Introduction to Thermostatistics* (Wiley, New York, 1985).
 - [3] B. Abou and F. Gallet, Probing a Nonequilibrium Einstein Relation in an Aging Colloidal Glass, *Phys. Rev. Lett.* **93**, 160603 (2004).
 - [4] K. Hayashi and S. Sasa, Effective temperature in nonequilibrium steady states of Langevin systems with a

- tilted periodic potential, *Phys. Rev. E* **69**, 066119 (2004).
- [5] J. Prost, J.-F. Joanny, and J. M. R. Parrondo, Generalized Fluctuation-Dissipation Theorem for Steady-State Systems, *Phys. Rev. Lett.* **103**, 090601 (2009).
- [6] T. Hatano and D. Jou, Measuring nonequilibrium temperature of forced oscillators, *Phys. Rev. E* **67**, 026121 (2003).
- [7] J. Ren and B. Li, Emergence and control of heat current from strict zero thermal bias, *Phys. Rev. E* **81**, 021111

- (2010).
- [8] P. Pradhan, C. P. Amann, and U. Seifert, Nonequilibrium Steady States in Contact: Approximate Thermodynamic Structure and Zeroth Law for Driven Lattice Gases, *Phys. Rev. Lett.* **105**, 150601 (2010).
 - [9] P. Pradhan, R. Ramsperger, and U. Seifert, Approximate thermodynamic structure for driven lattice gases in contact, *Phys. Rev. E* **84**, 041104 (2011).
 - [10] K. Kanazawa, T. Sagawa, and H. Hayakawa, Heat conduction induced by non-Gaussian athermal fluctuations *Phys. Rev. E* **87**, 052124 (2013).
 - [11] H. M. Jaeger, S. R. Nagel, and R. P. Behringer, Granular solids, liquids, and gases, *Rev. Mod. Phys.* **68**, 1259 (1996).
 - [12] I. S. Aranson and L. S. Tsimring, Patterns and collective behavior in granular media: Theoretical concepts, *Rev. Mod. Phys.* **78**, 641 (2006).
 - [13] T. Pöschel and T. Schwager, *Computational Granular Dynamics* (Springer, Berlin, 2005).
 - [14] N. V. Brilliantov and T. Pöschel, *Kinetic Theory of Granular Gases* (Oxford University Press, New York, 2010).
 - [15] S. F. Edwards, The Role of Entropy in the Specification of a Powder, in *Granular Matter: An Interdisciplinary Approach*, edited by A. Mehta (Springer-Verlag, New York, 1994), p. 121, and references therein.
 - [16] S. F. Edwards and R. B. S. Oakeshott, Theory of powders, *Phys. A (Amsterdam)* **157**, 1080 (1989).
 - [17] S. F. Edwards and D. V. Grinev, Statistical mechanics of vibration-induced compaction of powders, *Phys. Rev. E* **58**, 4758 (1998).
 - [18] H. A. Makse and J. Kurchan, Testing the thermodynamic approach to granular matter with a numerical model of a decisive experiment, *Nature* **415**, 614 (2002).
 - [19] R. Blumenfeld and S. F. Edwards, Granular Entropy: Explicit Calculations for Planar Assemblies, *Phys. Rev. Lett.* **90**, 114303 (2003).
 - [20] R. K. Bowles and S. S. Ashwin, Edwards entropy and compactivity in a model of granular matter, *Phys. Rev. E* **83**, 031302 (2011).
 - [21] G. Gradenigo, E. E. Ferrero, E. Bertin, and J.-L. Barrat, Edwards Thermodynamics for a Driven Athermal System with Dry Friction, *Phys. Rev. Lett.* **115**, 140601 (2015).
 - [22] D. Bi, S. Henkes, K. E. Daniels, and B. Chakraborty, The Statistical Physics of Athermal Materials, *Annu. Rev. Condens. Matter Phys.* **6**, 63 (2015).
 - [23] J. T. Jenkins and S. B. Savage, A theory for the rapid flow of identical, smooth, nearly elastic, spherical particles, *J. Fluid. Mech.* **130**, 187 (1983).
 - [24] J. T. Jenkins and M. W. Richman, Kinetic theory for plane shear flows of a dense gas of identical, rough, inelastic, circular disks, *Phys. Fluids* **28**, 3485 (1985).
 - [25] T.P.C. van Noije and M.H. Ernst, Velocity distributions in homogeneous granular fluids: the free and the heated case, *Granul. Matt.* **1**, 57 (1998).
 - [26] V. Garzó and J. W. Dufty, Dense fluid transport for inelastic hard spheres, *Phys. Rev. E* **59**, 5895 (1999).
 - [27] J. F. Lutsko, Transport properties of dense dissipative hard-sphere fluids for arbitrary energy loss models, *Phys. Rev. E* **72**, 021306 (2005).
 - [28] C. C. Maaß, N. Isert, G. Maret, and C. M. Aegerter, Experimental Investigation of the Freely Cooling Granular Gas, *Phys. Rev. Lett.* **100**, 248001 (2008).
 - [29] S. Tatsumi, Y. Murayama, H. Hayakawa, and M. Sano, Experimental study on the kinetics of granular gases under microgravity, *J. Fluid. Mech.* **641**, 521 (2009).
 - [30] GDR MiDi, On dense granular flows, *Eur. Phys. J. E* **14**, 341 (2004).
 - [31] Y. Forterre and O. Pouliquen, Flows of Dense Granular Media, *Annu. Rev. Fluid Mech.* **40**, 1 (2008).
 - [32] T. G. Sano and H. Hayakawa, Simulation of granular jets: Is granular flow really a perfect fluid?, *Phys. Rev. E* **86**, 041308 (2012).
 - [33] T. G. Sano and H. Hayakawa, Numerical analysis of impact processes of granular jets, *AIP Conf. Proc.* **1542**, 622 (2013).
 - [34] T. G. Sano and H. Hayakawa, Jet-induced jammed states of granular jet impacts, *Prog. Theor. Exp. Phys.* **(2013)** 103J02.
 - [35] X. Cheng, L. Gordillo, W. W. Zhang, H. M. Jaeger, and S. R. Nagel, Impact dynamics of granular jets with non-circular cross sections, *Phys. Rev. E* **89**, 042201 (2014).
 - [36] A. J. Liu and S. R. Nagel, Nonlinear dynamics: Jamming is not just cool any more, *Nature* **396**, 21 (1998).
 - [37] M. Otsuki and H. Hayakawa, Critical scaling near jamming transition for frictional granular particles, *Phys. Rev. E* **83**, 051301 (2011).
 - [38] H. Hayakawa and M. Otsuki, Nonequilibrium identities and response theory for dissipative particles, *Phys. Rev. E* **88**, 032117 (2013).
 - [39] K. Suzuki and H. Hayakawa, Divergence of Viscosity in Jammed Granular Materials: A Theoretical Approach, *Phys. Rev. Lett.* **115**, 098001 (2015).
 - [40] J. S. Olafsen and J. S. Urbach, Velocity distributions and density fluctuations in a granular gas, *Phys. Rev. E* **60**, R2468(R) (1999).
 - [41] A. Kudrolli and J. Henry, Non-Gaussian velocity distributions in excited granular matter in the absence of clustering, *Phys. Rev. E* **62**, R1489(R) (2000).
 - [42] G. W. Baxter and J. S. Olafsen, Kinetics: Gaussian statistics in granular gases, *Nature* **425**, 680 (2003).
 - [43] A. Kawarada and H. Hayakawa, Non-Gaussian Velocity Distribution Function in a Vibrating Granular Bed, *J. Phys. Soc. Jpn.* **73**, 2037-2040 (2004).
 - [44] J. J. Brey, M. J. Ruiz-Montero, and R. García-Rojo, Brownian motion in a granular gas, *Phys. Rev. E* **60**, 7174 (1999).
 - [45] A. Sarracino, D. Villamaina, G. Costantini, and A. Puglisi, Granular Brownian motion, *J. Stat. Mech.* **(2010)** P04013.
 - [46] K. Kanazawa, T. G. Sano, T. Sagawa, and H. Hayakawa, Minimal Model of Stochastic Athermal Systems: Origin of Non-Gaussian Noise, *Phys. Rev. Lett.* **114**, 090601 (2015).
 - [47] K. Kanazawa, T. G. Sano, T. Sagawa, and H. Hayakawa, Asymptotic Derivation of Langevin-like Equation with Non-Gaussian Noise and Its Analytical Solution, *J. Stat. Phys.* **160**, 1294 (2015).
 - [48] B. Cleuren and R. Eichhorn, Dynamical properties of granular rotors, *J. Stat. Mech.* **(2008)** P10011.
 - [49] J. Talbot, R. D. Wildman, and P. Viot, Kinetics of a Frictional Granular Motor, *Phys. Rev. Lett.* **107**, 138001 (2011).
 - [50] M. Smoluchowski, Zur kinetischen Theorie der Brownschen Molekularbewegung und der Suspensionen, *Annalen der Physik* **21**, 756 (1906).
 - [51] S. Chapman, On the Brownian displacements and thermal diffusion of grains suspended in a non-uniform fluid, *Proc. Roy. Soc. Ser. A* **119**, 34 (1928).

- [52] A. Kolmogorov, Ueber die analytischen Methoden in der Wahrscheinlichkeitsrechnung, *Math. Ann.* **104**, 415 (1931).
- [53] N. G. van Kampen, *Stochastic Processes in Physics and Chemistry*, 3rd ed. (North-Holland Personal Library, 2007).
- [54] C. Gardiner, *Stochastic Methods*, 4th ed. (Springer-Verlag, Berlin, 2009).
- [55] A. Naert, Experimental study of work exchange with a granular gas: The viewpoint of the Fluctuation Theorem, *Europhys. Lett.* **97**, 20010 (2012).
- [56] S. Joubaud, D. Lohse, and D. van der Meer, Fluctuation Theorems for an Asymmetric Rotor in a Granular Gas, *Phys. Rev. Lett.* **108**, 210604 (2012).
- [57] A. Gnoli, A. Puglisi, and H. Touchette, Granular Brownian motion with dry friction, *Europhys. Lett.* **102**, 14002 (2013).
- [58] A. Gnoli, A. Sarracino, A. Puglisi, and A. Petri, Nonequilibrium fluctuations in a frictional granular motor: Experiments and kinetic theory, *Phys. Rev. E* **87**, 052209 (2013).
- [59] A. Gnoli, A. Petri, F. Dalton, G. Pontuale, G. Gradenigo, A. Sarracino, and A. Puglisi, Brownian Ratchet in a Thermal Bath Driven by Coulomb Friction, *Phys. Rev. Lett.* **110**, 120601 (2013).
- [60] C.-É. Lecomte and A. Naert, Experimental study of energy transport between two granular gas thermostats, *J. Stat. Mech.* (**2014**) P11004.
- [61] A. Lorenz, C. Tuozzolo, and M.Y. Louge, Measurements of impact properties of small, nearly spherical particles, *Exp. Mech.* **37**, 292 (1997).
- [62] M. Louge (1999), Fall 1999 Impact Parameter Chart, <http://grainflowresearch.mae.cornell.edu/impact/data/ImpactParameterChart1999.pdf>.
- [63] J. T. Jenkins and C. Zhang, Kinetic theory for identical, frictional, nearly elastic spheres, *Phys. Fluids* **14**, 1228 (2002).
- [64] D. K. Yoon and J. T. Jenkins, Kinetic theory for identical, frictional, nearly elastic disks, *Phys. Fluids* **17**, 083301 (2005).
- [65] K. Saitoh and H. Hayakawa, Rheology of a granular gas under a plane shear, *Phys. Rev. E* **75**, 021302 (2007).
- [66] J. T. Jenkins and D. Berzi, Dense inclined flows of inelastic spheres: tests of an extension of kinetic theory, *Granul. Matt.* **12**, 151 (2010).
- [67] Y. Sone, *Molecular Gas Dynamics: theory, techniques, and applications* (Birkhäuser, Boston, 2007).
- [68] T. G. Sano and H. Hayakawa, Stochastic Mean Field Model of Heat Engine partitioned by Fluctuating Piston, arXiv: 1412.4468.
- [69] S.-S. Hsiau and W.-L. Yang, Stresses and transport phenomena in sheared granular flows with different wall conditions, *Phys. Fluids* **14**, 612 (2002).
- [70] D. van der Meer and P. Reimann, Temperature anisotropy in a driven granular gas, *Europhys. Lett.* **74**, 384 (2006).
- [71] D. J. Evans and G. P. Morriss, *Statistical Mechanics of Nonequilibrium Liquids* (Academic Press, London, 1990).
- [72] A. Puglisi, V. Loreto, U. Marini Bettolo Marconi, A. Petri, and A. Vulpiani, Clustering and Non-Gaussian Behavior in Granular Matter *Phys. Rev. Lett.* **81**, 3848 (1998).
- [73] T. P. C. van Noije, M. H. Ernst, E. Trizac, and I. Pagonabarraga, Randomly driven granular fluids: Large-scale structure, *Phys. Rev. E* **59**, 4326 (1999).
- [74] G. Gradenigo, A. Sarracino, D. Villamaina, and A. Puglisi, Non-equilibrium length in granular fluids: From experiment to fluctuating hydrodynamics, *Europhys. Lett.* **96**, 14004 (2011).
- [75] N. Khalil and V. Garzó, Homogeneous states in driven granular mixtures: Enskog kinetic theory versus molecular dynamics simulations, *J. Chem. Phys.* **140**, 164901 (2014).
- [76] B. N. J. Persson, *Sliding Friction* (Springer-Verlag, Berlin, 2000).
- [77] H. Hayakawa, Langevin equation with Coulomb friction, *Physica D* **205**, 48 (2005).
- [78] P. G. de Gennes, Brownian Motion with Dry Friction, *J. Stat. Phys.* **119**, 953 (2005).
- [79] T. Baumberger and C. Caroli, Solid friction from stick-slip down to pinning and aging, *Adv. Phys.* **55**, 279 (2006).
- [80] T. G. Sano and H. Hayakawa, Roles of dry friction in the fluctuating motion of an adiabatic piston, *Phys. Rev. E* **89**, 032104 (2014).
- [81] I. Eliazar and J. Klafter, Lévy-Driven Langevin Systems: Targeted Stochasticity, *J. Stat. Phys.* **111**, 739 (2003).
- [82] M. Abramowitz and I. A. Stegun, *Handbook of Mathematical Tables With Formulas, Graphs, and Mathematical Tables* (Dover, New York, 1964).
- [83] E. C. Titchmarsh, A pair of inversion formulae, *Proc. London Math. Soc.* **2**, 23 (1923).
- [84] G. Kuwabara and K. Kono, Restitution Coefficient in a Collision between Two Spheres, *Jpn. J. Appl. Phys.* **26**, 1230 (1987).
- [85] A. S. Bodrova, N. V. Brilliantov, and A. Yu. Loskutov, Brownian motion in granular gases of viscoelastic particles, *J. Exp. Theor. Phys.* **109**, 946 (2009).
- [86] C. Scalliet, A. Gnoli, A. Puglisi, and A. Vulpiani, Cages and Anomalous Diffusion in Vibrated Dense Granular Media, *Phys. Rev. Lett.* **114**, 198001 (2015).
- [87] J. Javier Brey, M. J. Ruiz-Montero, D. Cubero, and R. García-Rojo, Self-diffusion in freely evolving granular gases, *Phys. Fluids* **12**, 876 (2000).
- [88] H. Takahasi and M. Mori, Double Exponential Formulas for Numerical Integration, *Publications of RIMS, Kyoto University* **9**, 721 (1974).
- [89] G. E. Andrews, R. Askey, and R. Roy, *Special functions* (Cambridge University Press, Cambridge, England, 1999).